



## Stochastic simulation of cosmic ray modulation including a wavy heliospheric current sheet

K. Alanko-Huotari,<sup>1</sup> I. G. Usoskin,<sup>2</sup> K. Mursula,<sup>1</sup> and G. A. Kovaltsov<sup>3</sup>

Received 17 January 2007; revised 20 March 2007; accepted 15 April 2007; published 9 August 2007.

[1] We present a quasi-steady two-dimensional (axisymmetric) model of the heliospheric transport of galactic cosmic rays. The model is based on stochastic simulation techniques and includes all the modulation mechanisms that cosmic rays experience in the heliosphere: convection, adiabatic cooling, diffusion, and drifts. A special emphasis is given to the cosmic ray transport in the vicinity of the heliospheric current sheet (HCS), and a new method to calculate the wavy current sheet drift is presented. We study cosmic ray modulation in different solar modulation conditions and levels of waviness of the current sheet. We discuss changes in the cosmic ray spectrum and the dominant streaming patterns of cosmic rays in the heliosphere for different solar polarities and HCS tilt angles.

**Citation:** Alanko-Huotari, K., I. G. Usoskin, K. Mursula, and G. A. Kovaltsov (2007), Stochastic simulation of cosmic ray modulation including a wavy heliospheric current sheet, *J. Geophys. Res.*, 112, A08101, doi:10.1029/2007JA012280.

### 1. Introduction

[2] Galactic cosmic ray (GCR) modulation in the heliosphere has been intensively studied during the last decades. Still, there are some open questions, especially on the relative roles of different modulation mechanisms for different solar polarity and activity phases. Most modulation models are based on a solution of the transport equation of galactic cosmic rays developed by Parker [1965].

[3] The transport equation includes different modulation mechanisms that cosmic rays undergo on their travel in the heliosphere. Cosmic rays suffer from adiabatic energy losses in the expanding solar wind, diffusion on inhomogeneities of the heliospheric magnetic field (HMF), convection by the solar wind and drifts. Many methods have been developed to solve this equation numerically, most of them employing the finite difference technique [Jokipii and Levy, 1977; Burger and Potgieter, 1989; Scherer et al., 2002]. An alternative method is to reduce the problem from Parker's differential equation (which is of the Fokker-Planck type) to a set of ordinary differential equations that can be solved using the stochastic simulation technique, which has been successfully applied to various astrophysical problems (see section 3). This method allows to study processes, including those with unlimited derivatives (e.g., shocks), that cannot be easily considered by traditional methods. This method has been applied to heliospheric transport of cosmic rays in one-dimensional (1-D) case [Yamada et al., 1998; Gervasi et al., 1999b; Usoskin et al., 2002] and in 2-D case without the heliospheric current sheet (HCS) drift [Jokipii and Levy,

1977; Gervasi et al., 1999a; Alanko et al., 2003] or with a flat HCS [Zhang, 1999].

[4] Because of a clear difference in cosmic ray modulation in successive polarity periods, it is important to consider particle drifts [e.g., Jokipii and Levy, 1977; Isenberg and Jokipii, 1979]. Note that most earlier models include HCS drift as a  $\delta$ -function limit of the regular gradient drift [e.g., Jokipii et al., 1977; Jokipii and Thomas, 1981]. The results predict a stronger dependence of the GCR intensity on the HCS tilt angle for  $qA < 0$  than for  $qA > 0$  conditions [Potgieter and Moraal, 1985]. Another approach was used by Burger et al. [1985] who suggested that the HCS drift should not be treated as a  $\delta$ -function type modification in the gradient-curvature drift equations but needs to be extended to a region within 2 Larmor radii from the sheet. When applied to a wavy HCS, this leads to the effective drift "cone" [Burger and Potgieter, 1989]. It is widely recognized by now that drifts play a significant role in cosmic ray modulation, especially around solar activity minima. However, with increasing solar activity, other time-dependent phenomena, such as the propagating interaction regions, have a large contribution in modulation, and attempts trying to explain modulation by drift effects alone have not been very successful (see, e.g., reviews by Potgieter [1998], McDonald [1998], and Jokipii and Kóta [2000]).

[5] Although there are sophisticated, three-dimensional models of cosmic ray transport in the heliosphere [see, e.g., Kóta and Jokipii, 1983; Hattingh and Burger, 1995b], it is still useful to study periods of low solar activity with simpler models. We present here a steady-state, 2-D (axisymmetric) model of GCR transport, which can be used to study the drift-dominated modulation during low solar activity, when the heliospheric current sheet is well organized and the heliospheric conditions are fairly quiet. We first describe a new model to simulate the drift in the case of

<sup>1</sup>Department of Physical Sciences, University of Oulu, Oulu, Finland.

<sup>2</sup>Sodankylä Geophysical Observatory (Oulu unit), University of Oulu, Oulu, Finland.

<sup>3</sup>Ioffe Physical-Technical Institute, St. Petersburg, Russia.

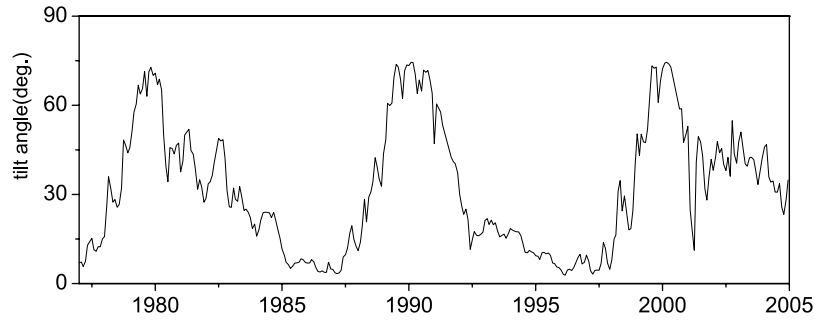


**Figure 1.** Heliospheric current sheet (HCS) tilt angle for the years 1977–2005.

a wavy current sheet and discuss some basic characteristics of the modelled drift velocity. We then describe our 2-D simulation model for GCR transport and discuss the results of the model for several situations.

## 2. Transport Equation

[6] The transport of cosmic rays in the heliosphere is described by Parker's equation which is of the Fokker-Planck type [Parker, 1965; Toptygin, 1985]. This equation includes the diffusion of particles along and perpendicular to the magnetic field lines, the gradient-curvature (regular) drift in the heliospheric magnetic field, the drift along the heliospheric current sheet, the convection with the solar wind, and the adiabatic energy losses in the expanding solar wind. For cosmic ray number density this equation can be written in the form [see, e.g., Parker, 1965; Burger and Potgieter, 1989]:

$$\frac{\partial U}{\partial t} = \nabla \cdot (\mathbf{K}^s \cdot \nabla U - \mathbf{V}_{sw} U - \langle \mathbf{v}_D \rangle U) + \frac{1}{3} (\nabla \cdot \mathbf{V}_{sw}) \frac{\partial}{\partial T} (aTU), \quad (1)$$

where  $U(T, \mathbf{r}, t)$  is the cosmic ray number density per unit interval of particle kinetic energy,  $T$ ;  $\mathbf{V}_{sw}$  is the solar wind speed;  $a = (T + 2 T_r)/(T + T_r)$  where  $T_r$  is the particle's rest energy (for a proton  $T_r = 0.938$  GeV);  $\mathbf{K}^s$  is the symmetric part of the diffusion tensor which contains diffusion coefficients along ( $\kappa_{\parallel}$ ) and perpendicular ( $\kappa_{\perp}$ ) to magnetic field lines.  $\langle \mathbf{v}_D \rangle$  is the drift velocity, averaged over the near-isotropic particle distribution, and includes the drift along the heliospheric current sheet,  $\langle \mathbf{v}_D \rangle_s$ , and the gradient-curvature drift in the regular heliospheric magnetic field,  $\langle \mathbf{v}_D \rangle_R$  [Jokipii and Thomas, 1981]. The drift velocity is usually considered as

$$\langle \mathbf{v}_D \rangle = \frac{1}{3} P v \nabla \times \left( \frac{\mathbf{B}}{B^2} \right), \quad (2)$$

where  $P$  and  $v$  are particle's rigidity and velocity, respectively, and  $\mathbf{B}$  is the regular magnetic field vector. We note that such a definition guarantees the divergence-free nature of drifts as requested by Liouville's theorem. Although the drifts per se cannot produce any CR modulation, they do affect the modulated GCR spectra by redirecting particles inside the heliosphere where the usual convection-diffusion modulation is present [e.g., Jokipii et al., 1977].

[7] In the present paper we assume Parker's magnetic field model [Parker, 1958] with a constant field at the Sun and a constant radial solar wind speed:

$$\mathbf{B}(r, \theta) = \frac{A}{r^2} (\mathbf{e}_r - \Gamma \mathbf{e}_{\phi}) \cdot (1 - 2H(\theta - \theta_s)), \quad (3)$$

where  $\Gamma = \tan \psi = \Omega r \sin \theta / V_{sw}$  corresponds to the angle  $\psi$  between the magnetic field and the radius vector,  $\Omega = 2.866 \cdot 10^{-6} \text{ s}^{-1}$  is the (sidereal Carrington) angular rotation rate of the Sun (rotation period is 25.38 days), and  $H$  is the Heavyside step function. Depending on the sign of  $A$  in equation (3), the magnetic field points either outward in the northern hemisphere ( $A > 0$ ) or inward ( $A < 0$ ). The polar angle of the heliospheric current sheet  $\theta_s$  can be written as [Jokipii and Thomas, 1981]:

$$\begin{aligned} \theta_s &= \frac{\pi}{2} + \sin^{-1} \left[ \sin \alpha \cdot \sin \left( \phi + \frac{r\Omega}{V_{sw}} \right) \right] \\ &\approx \frac{\pi}{2} + \alpha \sin \left( \phi + \frac{r\Omega}{V_{sw}} \right), \quad \text{for } \alpha \ll 1, \end{aligned} \quad (4)$$

where  $\alpha$  is the tilt angle of the sheet.

[8] The oppositely directed magnetic field lines confront at the heliomagnetic equator and a thin heliospheric current sheet is created in the interface of opposite polarities. The structure of the sheet strongly depends on the phase of the solar cycle. Since the magnetic axis of the Sun is tilted with respect to the rotational axis, the sheet produces a wavy structure, the so-called ballerina skirt. In an axisymmetric approximation the global HCS waviness is defined by the HCS tilt angle, which roughly corresponds to the tilt of the solar dipole axis with respect to the rotational axis. Figure 1 shows the variation of the HCS tilt angle for the time period 1976–2005. The tilt angle values are determined by Wilcox Solar Observatory (newer model, radial boundary condition). The drift velocity in the regular heliospheric magnetic field can be derived from equations (2) and (3) [see, e.g., Jokipii and Levy, 1977; Burger and Potgieter, 1989] and is directed equatorward (poleward) for  $qA > 0$  ( $qA < 0$ ).

[9] The HCS drift is caused by the reversal of the particle's Larmor gyration direction when it crosses the HCS. The drift motion is directed along the HCS and perpendicular to HMF. The HCS drift exists only in a narrow region around HCS, comparable to a few gyroradii. The HCS drift direction also depends on HMF polarity being toward (away) the Sun for  $qA < 0$  ( $qA > 0$ ).

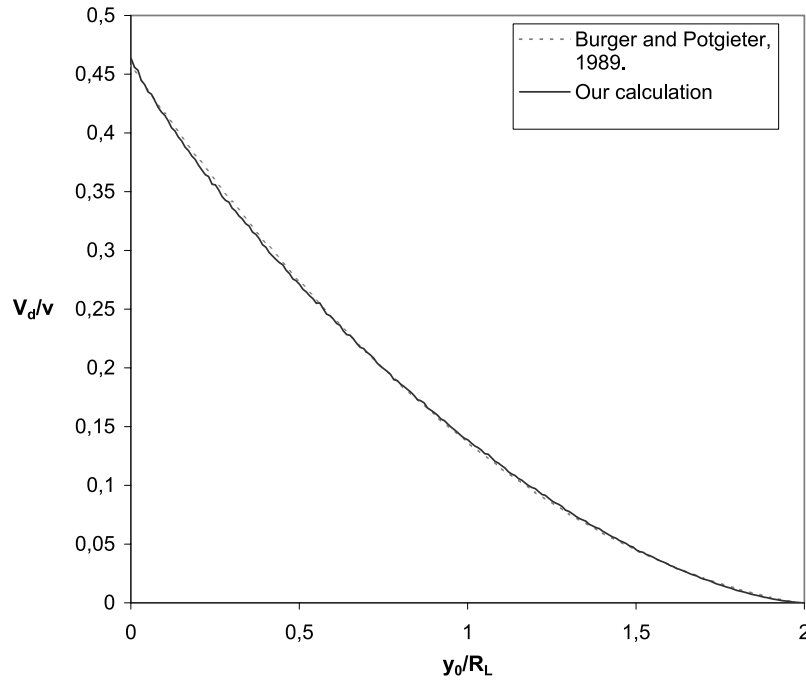


**Figure 2.** HCS drift velocity in the flat sheet.

[10] While the HCS drift is responsible mainly for the radial transport of GCRs around the ecliptic plane, the gradient-curvature drift operates in latitudinal direction all over the heliosphere. For  $qA < 0$ , the gradient-curvature drift drives particles from equatorial to polar regions leading to a loss of particles in the equatorial region. The HCS drift balances the effect of gradient-curvature drift by driving CR particles inward along the HCS. For  $qA > 0$  the situation is opposite. Thus the gradient-curvature drift and the HCS drift balance each other, in agreement with the divergence-free nature of the drift velocity field [cf. *Burger and Potgieter, 1989*]. Here we present a new way to include a wavy HCS drift into numerical models of CR transport in the heliosphere, developing the approach by *Burger et al. [1985]*.

### 2.1. Drift in a Flat Current Sheet

[11] Following *Burger et al. [1985]*, let us assume the GCR particle distribution around the HCS to be isotropic and the magnetic field to be homogeneous and of equal magnitude but of opposite directions on opposite sides of the sheet. Although equation (2) contains a  $\delta$ -function singularity at the sheet crossing, individual particles within two Larmor radii from the sheet experience a finite gradient drift either toward or away from the Sun, depending on solar polarity and the phase angle of the particle at the sheet crossing [e.g., *Burger et al., 1985*]. An equation giving the average relative HCS drift velocity of a particle takes the following form (a detailed calculation of the flat HCS drift can be found in the work of *Isenberg and Jokipii [1979]* and *Burger et al. [1985]*):

$$\frac{\langle v_D \rangle_S}{v} = \frac{1}{\pi} \int_0^1 \left[ \int \left( \frac{v_D}{v} \right) d\varphi \right] d\lambda, \quad (5)$$

where  $\lambda = \cos(\gamma)$ ,  $\gamma$  is the pitch angle of the particle, and  $\langle v_D \rangle_S$  is the HCS drift velocity,

$$\begin{cases} \frac{v_D}{v} = \frac{\sin(\eta)}{\eta} \sqrt{1 - \lambda^2} \\ \cos(\eta) = \sin(\varphi) - \frac{1}{\sqrt{1 - \lambda^2}} \left( \frac{L_0}{R_L} \right), \end{cases} \quad (6)$$

where  $\eta$  is the phase angle of the particle at the sheet crossing, and  $R_L$  and  $L_0$  are particle's Larmor radius and distance to the sheet, respectively. Limits of integration, over an auxiliary angle  $\varphi$ , for the inner term in equation (5) are determined by the condition  $|\cos(\eta)| \leq 1$ . Then the flat HCS drift velocity of equation (5) is given as

$$\langle v_D \rangle_S = \frac{A}{|A|} \langle v_D \rangle_S (\sin \psi \mathbf{e}_r + \cos \psi \mathbf{e}_\phi), \quad (7)$$

where  $\langle v_D \rangle_S$  can be numerically approximated as

$$\frac{\langle v_D \rangle_S}{v} = 0.4526 - 0.4034 \left( \frac{L_0}{R_L} \right) + 8.807 \cdot 10^{-2} \left( \frac{L_0}{R_L} \right)^2, \quad (8)$$

whenever  $(L_0/R_L) < 2$ . The maximum drift velocity of about  $0.45 v$  is achieved at the sheet and it rapidly decreases as the distance to the sheet increases. The resulting HCS drift velocity relative to the particle's velocity is shown in Figure 2.

[12] *Burger and Potgieter [1989]* suggested that the assumption of a homogeneous magnetic field along the HCS is justified only for particles with rigidity less than 10 GV. We found it unreasonable to cut the drifts off sharp at a specific rigidity as it produces unphysical breaks in the modulated CR energy spectra. Accordingly, we reduce the drifts gradually with increasing rigidity. Since high-energy

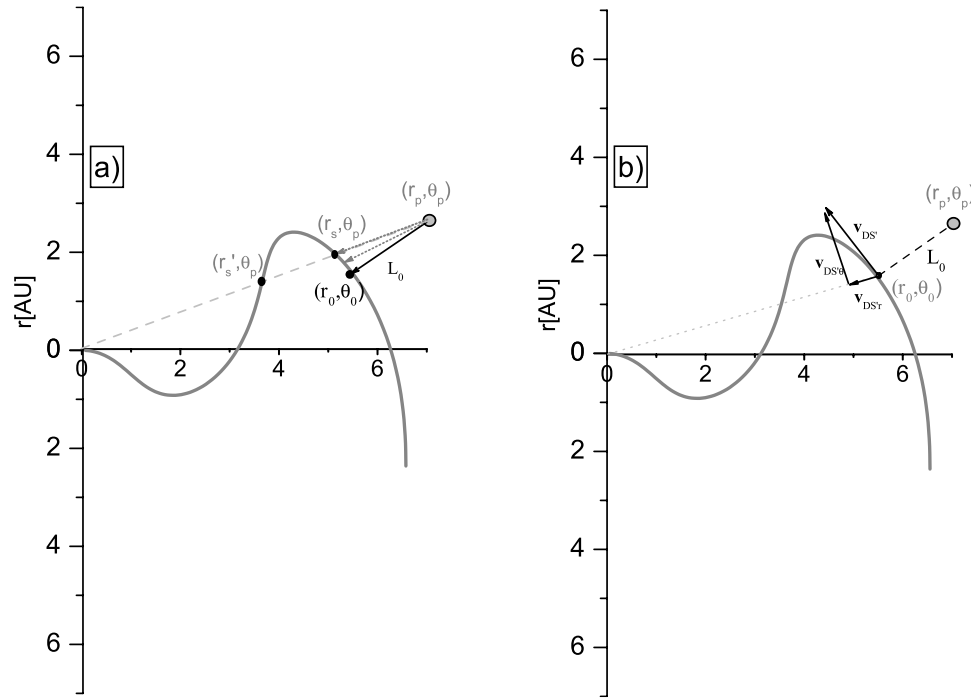


**Figure 3.** Heliospheric current sheet structure at a constant azimuth angle and with a  $30^\circ$  tilt angle. (a) Search for the minimum distance between the particle and the sheet. Coordinates  $(r_s, \theta_p)$  and  $(r'_s, \theta_p)$  show the possible starting points of the scan.  $(r_s, \theta_p)$  is chosen due to smaller distance to the particle's position  $(r_p, \theta_p)$ . (b) The drift velocity vector for a particle at position  $(r_p, \theta_p)$ .  $\mathbf{v}_{DS'}$  is the total HCS drift velocity vector,  $\mathbf{v}_{DS'r}$  and  $\mathbf{v}_{DS'\theta}$  are the radial and latitudinal components of  $\mathbf{v}_{DS'}$ , respectively.

particles ( $>100$  GV) should hardly experience any drift, while for low-energy particles ( $\sim 1$  GV) the drift effects are significant, we assumed that the region around the Sun where the GCR particles experience drifts depends on particle rigidity. We defined an “effective” drift region for a particle with rigidity  $P$  as

$$D_D = \frac{100AU}{(P/1GV)^n}, \quad (9)$$

where  $n$  is a free parameter.  $D_D$  defines the maximum distance from the Sun where the drift is still applied on GCR particles. Such a definition guarantees the validity of local HCS flatness approximation: particle's gyroradius  $L_0$  is smaller than the distance between HCS humps (about 6 AU). Note that the assumption of an effective drift region is a technical approach which only helps to reduce the drifts at higher rigidities and ensures a smooth converging of CR spectra. We have used  $n = 0.75$  but the exact value of this parameter is not crucially important.

## 2.2. Drift in a Wavy Current Sheet

[13] The assumption of a flat HCS is realistic only during the solar minimum when the current sheet tilt angle is small. From Figure 1 we see that the minimum value of the tilt angle, about 5 degrees, was reached in 1986–1987 and 1996–1997. Thus the flat sheet approximation is expected to be valid only for a couple of years per cycle. In order to study GCR intensity variations over longer timescales (wider solar activity range), a more realistic approach is to

study a wavy HCS with a larger tilt angle. It has been noted by many authors [e.g., Potgieter *et al.*, 1993; Le Roux and Potgieter, 1995] that the HCS drift and changing tilt angle can explain GCR variations during low solar activity but usually fail for moderate or strong solar activities. Also, when solar activity increases, the HCS structure gets more complicated and the assumption of a tilted HCS is an oversimplification. Since our model is 2-D and cannot model transient, time-dependent phenomena, we restrict our study to periods of low-to-moderate solar activity. This means tilt angles varying from 0 to about 40 degrees.

[14] Several methods have been presented to estimate the wavy HCS drift [Jokipii and Thomas, 1981; Burger and Potgieter, 1989; Hattingh and Burger, 1995a], all based on a various degree of simplification. Nevertheless, we present here a new way to numerically calculate the HCS drift for a wavy sheet. As the sheet has a 3-D structure, we need a way to simulate its effect in a 2-D axisymmetric model. We do this by studying the HCS drift at one longitude at a time and averaging the final result over all longitudes.

[15] First, we put a GCR particle to a position  $(r_p, \theta_p, \phi_p)$  inside the tilt cone and numerically find its minimum distance  $L_0$  to the sheet. A schematic view of the method is shown in Figure 3a. Although it is complicated to find the minimum distance to the sheet (point  $(r_0, \theta_0)$ ), it is relatively easy to find the closest point on the sheet with the same polar angle  $\theta_s = \theta_p$  at the fixed longitude. Then we calculate the sheet's radial coordinate with equation (4), when  $\theta_p$  and  $\phi_p$  are fixed. We find the particle's minimum distance to the sheet by scanning all the distances between the particle and

the sheet. If the particle is above (below) the sheet, the minimum distance will be found when scanning downward (upward) along the sheet. Once we have defined the scanning direction, we change slightly the polar angle  $\theta_s$  to the direction of the scan, find the position of the sheet at this new polar angle, and calculate the distance to the particle. Comparing the new distance to the reference distance, we continue this procedure until the minimum distance  $L_0$  has been found. In a realistic 3-D geometry the shortest way to HCS may lie off the  $\theta - r$  plane, and our procedure can overestimate the minimum distance. However, we have checked that a possible error does not exceed 1% for  $r > 6$  AU, 10% for 2 AU and becomes greater only in the vicinity of the Sun ( $< 10^{-5}$  of the heliosphere's volume).

[16] Once we have found the minimum distance between the particle and the sheet, we are ready to calculate the actual drift velocity of the particle for current longitude using the locally quasi-flat sheet approach. The direction and magnitude of the HCS drift velocity are achieved using the information that it is tangential to the sheet. If the scanning direction is away from the Sun, taking the direction from the second last scanning point to the last one gives the direction of  $\mathbf{v}_{DS}$  ( $-\mathbf{v}_{DS}$ ) for  $qA > 0$  ( $qA < 0$ ) case. If the scanning direction is toward the Sun, an inverse approach is applied. If we now assume the sheet to be locally flat (as guaranteed by equation (9)), with the information of particle's Larmor radius and distance to the sheet we can apply equation (8) and calculate the magnitude of the drift vector.

[17] The heliospheric magnetic field is bent to a spiral, and the effective HCS drift velocity direction changes with radial distance. The HCS drift takes place in a plane perpendicular to the magnetic field direction. Far away from the Sun, the spiral angle is close to  $90^\circ$  and the HCS drift direction is directly toward the Sun for  $qA < 0$ . However, in the inner heliosphere, where the spiral angle is smaller, the azimuthal component of the drift velocity dominates and the drift velocity toward the Sun is rather small. We take this into account simply by multiplying the drift velocity by  $\sin \psi$ , where  $\psi$  is the spiral angle. The corresponding velocity vector is denoted as  $\mathbf{v}_{DS}$ .

[18] Finally, we need to find the radial and latitudinal component of the drift vector (the azimuthal components of the HCS drift does not play a role in our 2-D model). Figure 3b shows the determination of  $\mathbf{v}_{DS}$  and its radial and latitudinal components. We denote the angle between  $\mathbf{v}_{DS}$  and  $\mathbf{v}_{DSr}$  as  $\xi$ . Thus the radial and latitudinal components of  $\mathbf{v}_{DS}$  are defined as (see Figure 3b):

$$v_{DSr} = \cos(\xi)v_{DS} \quad (10)$$

$$v_{DS\theta} = \sin(\xi)v_{DS}. \quad (11)$$

[19] Now we have all the necessary information to calculate the particle's drift velocity at the position  $(r_p, \theta_p, \phi_p)$ . Next we slightly change the longitude and calculate the corresponding HCS drift velocity vector. We repeat this procedure covering all longitudes, then sum up the radial and latitudinal components of the drift velocity vector and average the result.

[20] We find that the average latitudinal component of the HCS drift velocity is negligible with respect to the radial component. Thus we apply only the radial component of the HCS drift velocity in our modulation model and call it here simply the HCS drift velocity. We calculated the HCS drift velocity inside the HCS tilt cone for particles with rigidities between 1 GV and 100 GV,  $r_p$  varying from 1 AU to the heliospheric boundary at 100 AU, with a grid size of 1 AU in radial and  $0.1\alpha$  in latitudinal direction.

[21] Figure 4 shows an example of a 9 GV and a 2 GV proton's drift velocity in a HCS with the tilt angle  $\alpha = 2^\circ$  and  $40^\circ$ . Figure 4 shows that for a relatively energetic particle (9 GV) the HCS drift velocity in the inner heliosphere increases with the radial distance, reaches its maximum at the distance of about 5–10 AU, and decreases in the outer heliosphere. For the lower-energy particle the drift velocity stays roughly constant with radial distance. In most cases the drift velocity increases with latitude and reaches maximum at the edge of the tilt cone. Interestingly, this is not the case for relatively energetic particles with very small tilt angles. As seen from Figure 4a, for a 9 GV particle in a sheet with  $2^\circ$  tilt angle the radial dependence of the drift velocity is rather weak at the edge of the tilt cone and strong at equator. This results in a situation where the drift velocity in the inner heliosphere is highest in equatorial plane and decreases with latitude. This behavior, however, is reversed around 30–40 AU, where the drift velocity becomes larger for higher latitudes. When the particle energy increases, the drift velocity in the inner heliosphere at the edge of the tilt cone approaches the drift velocity at equator. It should be studied further whether this exception is a real result or a computational artifact related to the very low tilt angle. The larger is the particle energy, the larger is also the drift velocity relative to particle's velocity. For a 9 GV proton in a sheet with  $2^\circ$  tilt angle the maximum drift velocity is about  $0.3 v$  at 5–10 AU distance, while for a 2 GV particle it is only about  $0.10 v$ . With  $40^\circ$  tilt angle the drift velocity is only few percent of the particle velocity at most.

### 3. Basic 2-D Stochastic Simulation Model

[22] The heliosphere is essentially nonaxisymmetric at every moment, and 3-D models are needed for detailed studies on short timescales. On the other hand, it is usual to study long-term cosmic ray modulation using 2-D (axisymmetric) models, where all longitudinal effects are averaged. In the axisymmetric case, Parker's transport equation (equation (12)) takes the following form:

$$\begin{aligned} \frac{\partial U}{\partial t} = & \frac{1}{r^2} \frac{\partial}{\partial r} \left( r^2 \kappa_{rr} \frac{\partial U}{\partial r} \right) + \frac{1}{r^2} \frac{\partial}{\partial \mu} \left( (1 - \mu^2) \kappa_{\theta\theta} \frac{\partial U}{\partial \mu} \right) \\ & - \frac{1}{r^2} \frac{\partial}{\partial r} \left( r^2 \left( V_{sw} + \langle v_D \rangle_{R_r} + \langle v_D \rangle_{S_r} \right) U \right) \\ & - \frac{1}{r} \frac{\partial}{\partial \mu} \left( \sqrt{1 - \mu^2} \langle v_D \rangle_{R_\theta} U \right) + \frac{2 V_{sw}}{3 r} \frac{\partial}{\partial T} (aTU), \end{aligned} \quad (12)$$

where  $\mu = \cos\theta$ , and  $\kappa_{rr} = \kappa_{\parallel} \cos^2\psi + \kappa_{\perp} \sin^2\psi$  and  $\kappa_{\theta\theta} = \kappa_{\perp}$  are the diffusion coefficients in radial and latitudinal direction, respectively.

[23] This transport equation can be solved by the stochastic simulation method as follows. Introducing a new

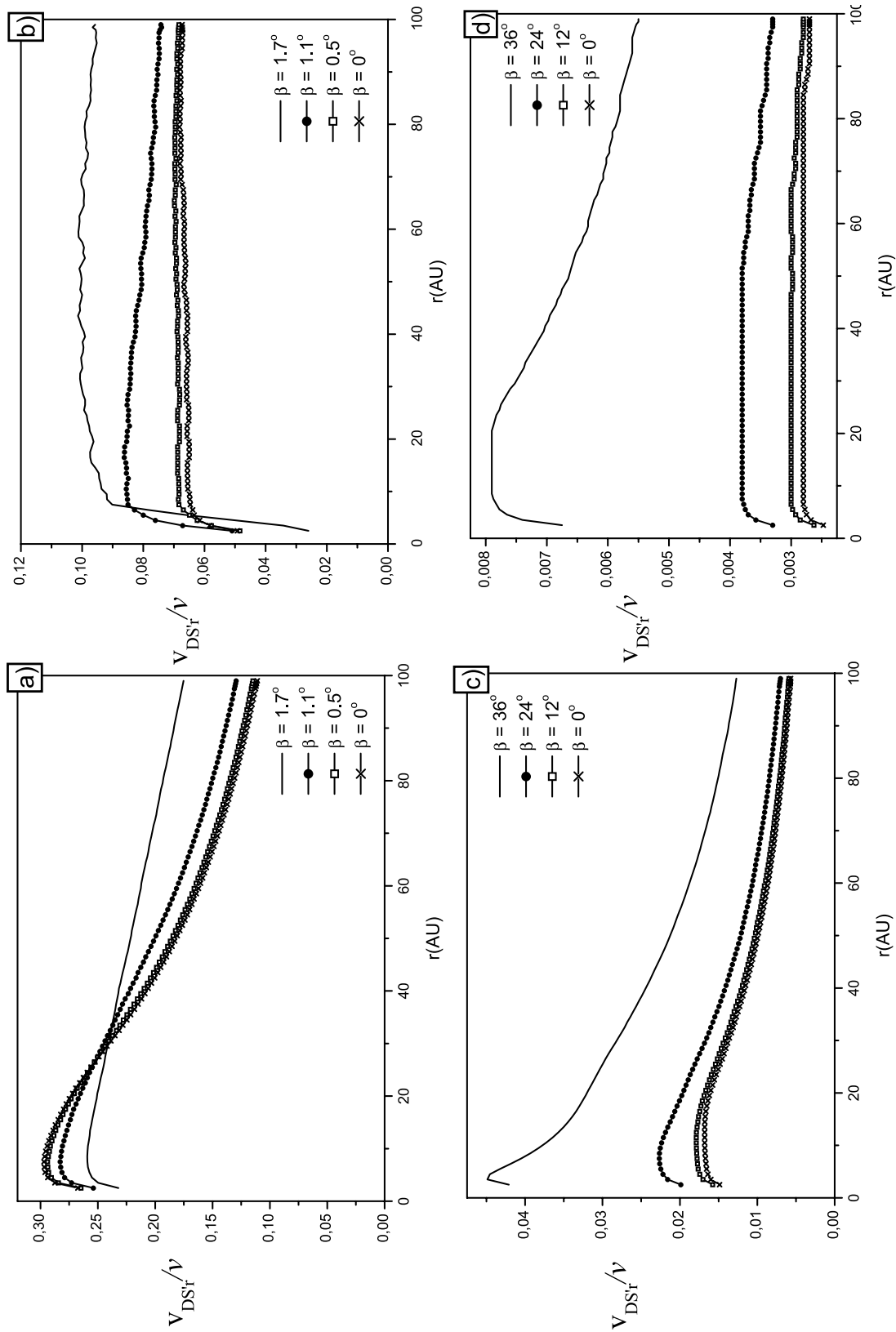


**Figure 4.** HCS drift velocity in a case of (a) HCS tilt angle  $\alpha = 2^\circ$  and  $P = 9$  GV, (b)  $\alpha = 2^\circ$  and  $P = 2$  GV, (c)  $\alpha = 40^\circ$  and  $P = 9$  GV, (d)  $\alpha = 40^\circ$  and  $P = 2$  GV.  $\beta$  denotes the latitude.

function  $F = r^2 U$ , one can transform equation (12) into the following form:

$$\begin{aligned} \frac{\partial F}{\partial t} = & \frac{\partial^2}{\partial r^2} (\kappa_{rr} F) - \frac{\partial}{\partial r} \left( \frac{1}{r^2} \frac{\partial (r^2 \kappa_{rr})}{\partial r} F \right) \\ & - \frac{\partial}{\partial r} \left( (V_{sw} + \langle v_D \rangle_{R_r} + \langle v_D \rangle_{S_r}) F \right) \\ & + \frac{\partial^2}{\partial \mu^2} \left( \frac{1}{r^2} (1 - \mu^2) \kappa_{\theta\theta} F \right) - \frac{\partial}{\partial \mu} \left( \frac{1}{r^2} \frac{\partial ((1 - \mu^2) \kappa_{\theta\theta})}{\partial \mu} F \right) \\ & + \frac{\partial}{\partial \mu} \left( \frac{1}{r} \sqrt{1 - \mu^2} \langle v_D \rangle_{R_\theta} F \right) \\ & + \frac{\partial}{\partial T} \left( \frac{2}{3} \frac{V_{sw}}{r} a T F \right). \end{aligned} \quad (13)$$

[24] This equation can be presented as an equivalent set of stochastic differential equations [Gardiner, 1989]

$$\begin{aligned} \Delta r = & \frac{1}{r^2} \frac{\partial}{\partial r} (r^2 \kappa_{rr}) \Delta t + (V_{sw} + \langle v_D \rangle_{R_r} + \langle v_D \rangle_{S_r}) \Delta t \\ & + R_{n1} \sqrt{2 \kappa_{\theta\theta}} \Delta t \\ \Delta \mu = & \frac{1}{r^2} \frac{\partial}{\partial \mu} ((1 - \mu^2) \kappa_{\theta\theta}) \Delta t - \frac{\sqrt{1 - \mu^2}}{r} \langle v_D \rangle_{R_\theta} \Delta t \\ & + R_{n2} \sqrt{\frac{2}{r^2} (1 - \mu^2) \kappa_{\theta\theta}} \Delta t \\ \Delta T = & -\frac{2}{3} \frac{V_{sw} a T}{r} \Delta t, \end{aligned} \quad (14)$$

where  $R_{n1}$  and  $R_{n2}$  are normally distributed random numbers with unit dispersion. The components of the drift velocity in a regular heliospheric magnetic field can be derived from equations (2) and (3) [cf. Jokipii and Levy, 1977; Burger and Potgieter, 1989]:

$$\langle v_D \rangle_{R_r} = -\frac{2}{3} \frac{Pv}{A} \frac{r \Gamma \cos \theta}{\sin \theta (1 + \Gamma^2)^2} (1 - 2H(\theta - \theta_s)) \quad (15)$$

$$\langle v_D \rangle_{R_\theta} = \frac{2}{3} \frac{Pv}{A} \frac{r \Gamma (2 + \Gamma^2)}{(1 + \Gamma^2)^2} (1 - 2H(\theta - \theta_s)) \quad (16)$$

[25] In this study we have used the following assumptions. The solar wind speed was taken constant at  $V_{sw} = 400$  km/s. The diffusion coefficients are defined as follows [Kóta and Jokipii, 1983]:

$$\kappa_{\parallel} = \kappa_0 K(P) \frac{B_0}{3B} \quad (17)$$

$$\kappa_{\perp} = (\kappa_{\perp})_0 \kappa_{\parallel}, \quad (18)$$

where  $K(P) = 1$  GV, if  $P < 1$  GV, and  $K(P) = P$ , if  $P \geq 1$  GV [e.g., Perko, 1987].  $B_0 = 5$  nT is the mean magnetic field strength at the Earth's orbit, and  $B$  results from equation (3) with  $|A| = 3.4$  nT · AU<sup>2</sup>.

[26] A relation between the diffusion coefficients perpendicular and parallel to the magnetic field is often assumed to be linear with the proportionality coefficient  $(\kappa_{\perp})_0$  (see equation (18)). The value of  $(\kappa_{\perp})_0$  is usually taken between

0.01 and 0.05 [e.g., Kóta and Jokipii, 1983; Giacalone and Jokipii, 1999]. In this study we use  $(\kappa_{\perp})_0 = 0.04$ . Despite such a seemingly preferable parallel diffusion, the cosmic ray transport is mostly defined by perpendicular diffusion in the outer heliosphere, and parallel diffusion plays a role only in the inner heliosphere.

[27] The cosmic ray energy spectrum outside the heliosphere, i.e., the unmodulated spectrum (the local interstellar spectrum, LIS) is assumed constant. The exact shape of LIS is not well known. Here we use LIS adopted from Burger et al. [2000] in the form parameterized by Usoskin et al. [2005]:

$$J_{LIS}(P) = \frac{1.9 \times 10^4 \cdot P^{-2.78}}{1 + 0.4866 \cdot P^{-2.51}}, \quad (19)$$

where  $P = \sqrt{T(T + 2 \cdot 0.938)}$ ,  $J$  and  $T$  are expressed in units of particles/(m<sup>2</sup> sr s GeV/nucleon) and in GeV/nucleon, respectively.

[28] The set of stochastic equations (14) was numerically solved as the history of a quasi-particle with coordinates  $r$  and  $\theta$  and kinetic energy  $T$  in subsequent small time steps  $\Delta t$ . Collecting large statistics ( $>10^6$ ) of thus traced “particles,” we can finally obtain spatial and energy distributions of cosmic rays. The heliospheric spherical boundary was placed at 100 AU, and test particles were injected at the distance of 120 AU with the initial kinetic energy  $T$  distributed according to  $J_{LIS}$  (see equation (19)). Particle tracing was done by calculating the new coordinates and energy (see equation (14)) of the particle after a time step  $\Delta t$ , which was taken to depend on the heliodistance as  $\Delta t \propto r^2$  to reduce the computation time. The particle's history was terminated if it left the heliosphere or if its rigidity decreased below 1 GV. Some simulation results are presented in the following section.

## 4. Simulation Results

### 4.1. Flat Current Sheet

[29] Let us first discuss the case of minimum solar activity when the heliospheric current sheet is very flat and modulation quite weak. We set the diffusion coefficient to  $\kappa_0 = 8.8 \cdot 10^{-7}$  AU<sup>2</sup>s<sup>-1</sup> GV<sup>-1</sup> and applied the flat HCS of equation (8). We calculated the modulated cosmic ray spectrum both for  $qA < 0$  and  $qA > 0$  cases, as well as for the case without any drifts. The results are shown in Figure 5a. The spectrum in the  $qA < 0$  case is less modulated than for  $qA > 0$  or in the no-drift case, and the no-drift spectrum lies between  $qA < 0$  and  $qA > 0$ .

### 4.2. Wavy Current Sheet

[30] First, we tested our way to calculate the wavy current sheet drift discussed in section 2.2. Figure 5b shows simulated spectra with  $\kappa_0 = 3.0 \cdot 10^{-7}$  AU<sup>2</sup> s<sup>-1</sup> GV<sup>-1</sup> (which in no-drift case corresponds to relatively low modulation conditions), both for  $qA < 0$  and  $qA > 0$ , applying the flat sheet approximation and the wavy current sheet approximation with different tilt angles. We see that the spectra for the flat sheet case and the  $\alpha = 2^\circ$  case are fairly close to each other with both polarities, as one would expect. For tilt angles  $\alpha = 25^\circ$  and  $40^\circ$ , the spectra for  $qA < 0$  are less modulated than for  $qA > 0$ . In  $qA < 0$  case, modulation is weaker for  $\alpha = 2^\circ$  than for  $\alpha = 25^\circ$  and  $40^\circ$ ,

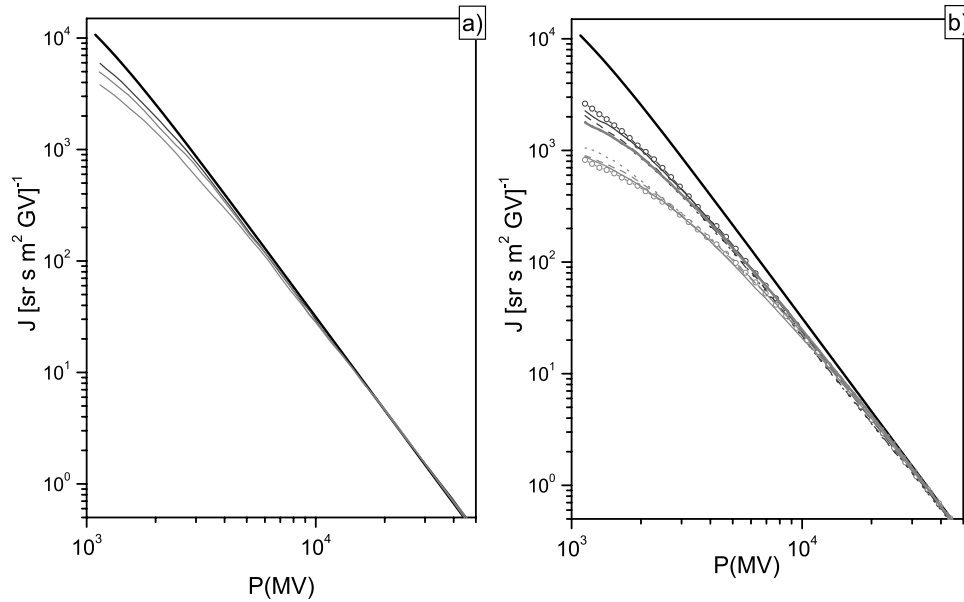


**Figure 5.** Simulated GCR spectra in case of (a) low solar modulation with flat HCS: LIS (thick black line),  $qA < 0$  (blue line),  $qA > 0$  (red line), and no-drift case (grey line) (b) relatively low solar modulation with flat and wavy HCS: LIS(thick black line),  $qA < 0$  with (1) flat HCS (blue dots), (2) wavy HCS with  $\alpha = 2^\circ$  (solid blue line), (3)  $\alpha = 25^\circ$  (dashed blue line), (4)  $\alpha = 40^\circ$  (dotted blue line), and  $qA > 0$  with (1) flat HCS (red dots), (2) wavy HCS with  $\alpha = 2^\circ$  (solid red line), (3)  $\alpha = 25^\circ$  (dashed red line), (4)  $\alpha = 40^\circ$  (dotted red line), and no-drift case(grey line).

which are very close to each other. This implies a tilt angle dependence (for relatively small tilt angles) of the GCR intensity at the Earth's orbit in  $qA < 0$  conditions. This feature is observed in neutron monitor data as peak-like profiles of the GCR intensity around solar activity minima for  $qA < 0$ . Our results also suggest that the HCS effect quickly decreases with increasing  $\alpha$  and approaches the no-drift case, which is in agreement with other studies [see, e.g., *Dorman, 2006*, and references therein]. We note that our simulation results are consistent with the features observed in neutron monitor data. The tilt angle dependence of modulation is weak for small values of  $\alpha$  during  $qA > 0$  period, in agreement with a flat top and fast ascend/descend of a  $qA > 0$  cycle in NM data. The tilt angle dependence is stronger for  $qA < 0$  periods, in agreement with the sharp tops of the corresponding cycles in NM data. On the other hand, the overall stronger modulation in  $qA > 0$  period shown by our results is different from earlier expectations [e.g., *Dorman, 2006*, and references therein], and this needs further, more detailed, investigation.

### 4.3. Streaming of GCR Particles

[31] Using stochastic simulation, one can study streaming patterns of cosmic rays in the heliosphere. In order to do this, we divided the 2-D heliosphere into cells of equal size of  $4 \text{ AU} \times 4 \text{ AU}$ . We studied the cases of  $\alpha = 2^\circ$  and  $40^\circ$ , and the two polarities. We traced a large set of particles with initial rigidity of  $P = 2 \text{ GV}$  (keeping diffusion coefficient at  $\kappa_0 = 3.0 \cdot 10^{-7} \text{ AU}^2 \text{ s}^{-1} \text{ GV}^{-1}$ ). Each time a particle left a cell, we recorded its “velocity” components  $v_x = \Delta x / \Delta t$  and  $v_y = \Delta y / \Delta t$ . Then the streaming pattern was computed by averaging over the whole set of  $v_x$  and  $v_y$  in each cell. This averaged streaming component is shown in Figure 6.

One can see that the streaming patterns are highly organized but quite different for  $qA < 0$  and  $qA > 0$ . In  $qA > 0$  conditions (see Figures 6a and 6c) the particle streaming around the HCS is preferably oriented equatorward due to the gradient-curvature drift. In  $\alpha = 2^\circ$  case the drift along the HCS is quite strong, and the particles preferably escape from the heliosphere along the sheet. In the  $\alpha = 40^\circ$  case the HCS drift velocity is quite small as discussed in section 2.2. Thus the HCS effect is weak and the gradient-curvature drift seems to dominate even at low latitudes. This could explain why the modulation decreases in  $qA > 0$  period with increasing tilt angle.

[32] In  $qA < 0$  conditions (see Figures 6b and 6d) the gradient-curvature drift causes poleward streaming of particles, especially at high latitudes. At equatorial regions the HCS drift dominates in  $\alpha = 2^\circ$  case and the particles are effectively driven toward the Sun. However, for  $\alpha = 40^\circ$  only a small oppositely oriented HCS effect can be seen due to the low HCS drift velocity.

## 5. Conclusions

[33] We have presented a 2-D, quasi-steady state model of GCR transport in the heliosphere, based on the stochastic simulation technique. A special emphasis is paid to the effect of drifts on the GCR transport. We have first discussed an analytical approach to the flat HCS drift and then presented a detailed numerical recipe of computing wavy HCS effect, calculating the HCS drift velocity at a fixed position of a GCR particle with a rigidity  $P$  and HCS tilt angle  $\alpha$ . The local HCS drift velocity at a fixed longitude is averaged over all longitudes. The drift velocity is found to increase with particle's energy and to decrease with increas-

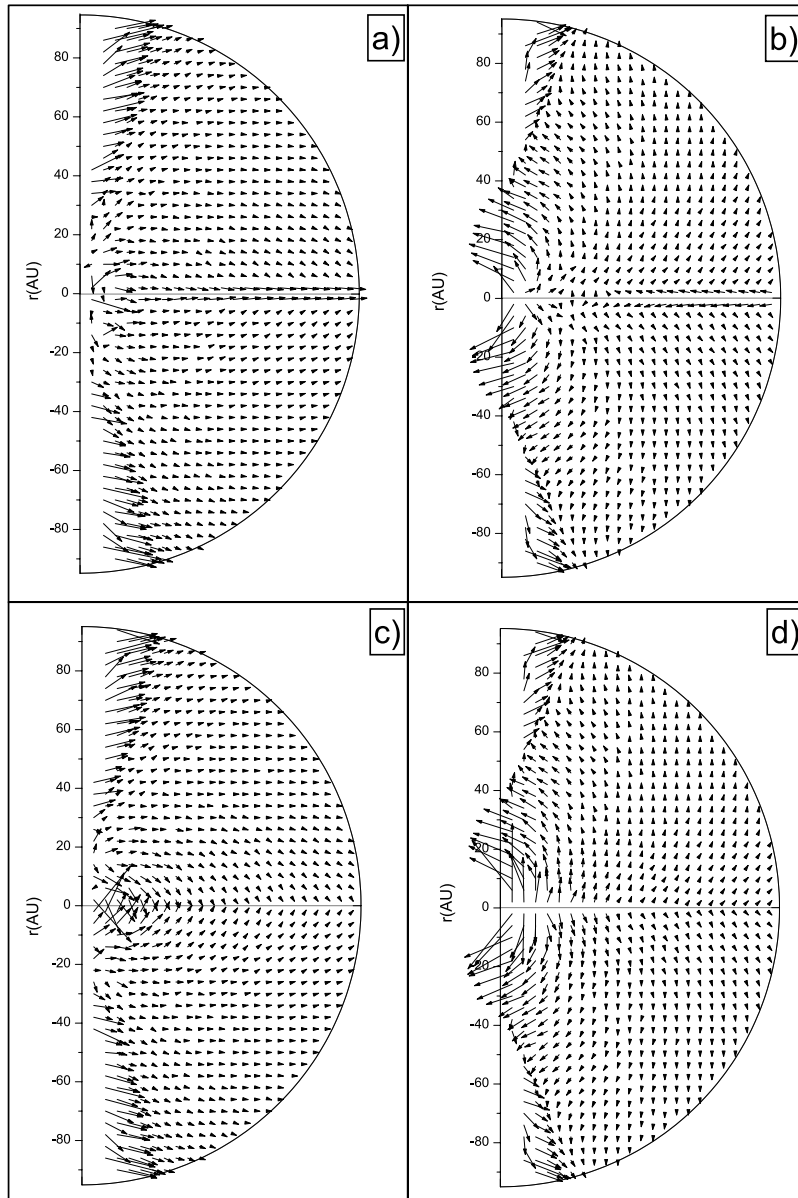


**Figure 6.** Streaming patterns of 2 GV particles in relatively low modulation conditions ( $\kappa_0 = 3.0 \cdot 10^{-7} \text{ AU}^2 \text{ s}^{-1} \text{ GV}^{-1}$ ) in (a)  $qA > 0$  period with  $\alpha = 2^\circ$ , (b)  $qA < 0$  period with  $\alpha = 2^\circ$ , (c)  $qA > 0$  period with  $\alpha = 40^\circ$ , (d)  $qA < 0$  period with  $\alpha = 40^\circ$ .

ing tilt angle. In most cases, the drift velocity also increases with increasing latitude. An exception to this is found for very low tilt angles ( $\alpha = 2^\circ$ ) for relatively energetic particles, when the drift velocity in the inner heliosphere is somewhat larger at lower latitudes, but this may be related to the statistical uncertainty of the simulations. In the radial direction, the HCS drift velocity for energetic particles increases first with increasing distance from the Sun, reaching its maximum around 5–10 AU, and then gradually decreases. For low-energy particles the drift velocity stays roughly constant with radial distance.

[34] We have applied both the flat and wavy current sheet in the full 2-D model. We have simulated the effect of HCS drift in a wide range of parameters: from low to medium modulation and from flat to wavy HCS. Our results are consistent with observations and verify that GCR modula-

tion is stronger for  $qA > 0$ . For  $qA < 0$ , the HCS drift advances the particle transport into the inner heliosphere, decreasing modulation with respect to nondrift case and especially to  $qA > 0$  case. Modulation increases with the tilt angle for  $qA < 0$  to some extent, but then the spectra seem to approach the nondrift case, which serves as an upper limit of modulation for  $qA < 0$ . The increase of modulation with the tilt angle for  $qA < 0$  is in agreement with earlier studies [see, e.g., *Kóta and Jokipii, 1983; Burger and Potgieter, 1989*]. For  $qA > 0$  conditions increasing tilt angle diminishes the modulation slightly.

[35] We also studied streaming patterns of GCR particles of 2 GV rigidity for low-to-moderate modulation conditions. In  $qA > 0$  case, the main pattern is that for a flat HCS the particles are driven by the gradient-curvature drift equatorward and away from the Sun by the HCS drift. For  $qA < 0$ ,

the particles are driven along the HCS toward the Sun and poleward by the gradient-curvature drift. With large tilt angle, the HCS effect is minor compared to the gradient-curvature drift, which dominates the whole heliosphere. The streaming patterns are in qualitative agreement with the common idea of GCR transport that in  $qA < 0$  period particles drift toward the poles in off-equatorial regions and toward the Sun in ecliptic plane, and the situation is reversed in  $qA > 0$  period [e.g., Jokipii and Thomas, 1981].

[36] More detailed calculations are needed to study, e.g., the effect of the applied concept of “drift region,” and the effect of the choice of  $(\kappa_{\perp})_0$  and  $\kappa_0$ . Another step could be to use a more realistic latitudinal dependence of the solar wind velocity, which was taken to be constant. An important application of the model is to compare the model results to the actual cosmic ray measurements, i.e., to the neutron monitor count rates. This requires, however, lengthy calculations where the diffusion coefficient  $(\kappa_{\perp})_0$  and tilt angle  $\alpha$  are changed as a function of time.

[37] **Acknowledgments.** The Finnish Graduate School in Astronomy and Space Physics and the Academy of Finland are acknowledged for financial support. We thank the Wilcox Solar Observatory for the HCS tilt angle data.

[38] Zuyin Pu thanks the reviewers for their assistance in evaluating this paper.

## References

- Alanko, K., I. G. Usoskin, K. Mursula, and G. A. Kovaltsov (2003), A 2D stochastic simulation of galactic cosmic rays transport in the heliosphere, *Proc. Int. Conf. Cosmic Rays 28th*, 7, 3851–3854.
- Burger, R. A., and M. S. Potgieter (1989), The calculation of neutral sheet drift in two-dimensional cosmic-ray modulation models, *Astrophys. J.*, 339, 501–511.
- Burger, R. A., H. Moraal, and G. M. Webb (1985), Drift theory of charged particles in electric and magnetic fields, *Astrophys. Space Sci.*, 116, 107–129.
- Burger, R. A., M. S. Potgieter, and B. Heber (2000), Rigidity dependence of cosmic ray proton latitudinal gradients measured by the Ulysses spacecraft: Implications for the diffusion tensor, *J. Geophys. Res.*, 105, 27,447–27,456.
- Dorman, L. (2006), *Cosmic Ray Interactions, Propagation, and Acceleration in Space Plasmas*, Springer, Dordrecht, Netherlands.
- Gardiner, C. W. (1989), *Handbook of Stochastic Methods*, Springer Verlag, Berlin.
- Gervasi, M. P., G. Rancoita, and I. G. Usoskin (1999a), Transport of galactic cosmic rays in the heliosphere: Stochastic simulation approach, *Proc. Int. Conf. Cosmic Rays 26th*, 7, 69–72.
- Gervasi, M., P. G. Rancoita, I. G. Usoskin, and G. A. Kovaltsov (1999b), Monte-Carlo approach to galactic cosmic ray propagation in the heliosphere, *Nucl. Phys. B*, 78, proc. suppl., 26–31.
- Giacalone, J., and J. R. Jokipii (1999), The transport of cosmic rays across a turbulent magnetic field, *Astrophys. J.*, 520, 204–214.
- Hattingh, M., and R. A. Burger (1995a), A new simulated wavy neutral sheet drift model, *Adv. Space Res.*, 16(9), 213–216.
- Hattingh, M., and R. A. Burger (1995b), Some properties of a fully three-dimensional drift model for the modulation of galactic cosmic rays, *Proc. Int. Conf. Cosmic Rays 24th*, 4, 337–340.
- Isenberg, P. A., and J. R. Jokipii (1979), Gradient and curvature drifts in magnetic fields with arbitrary spatial variation, *Astrophys. J.*, 234, 746.
- Jokipii, J. R., and J. Kóta (2000), Galactic and anomalous cosmic rays in the heliosphere, *Astrophys. Space Sci.*, 274, 77–96.
- Jokipii, J. R., and E. H. Levy (1977), Effects of particle drifts on the solar modulation of galactic cosmic rays, *Astrophys. J.*, 213, L85–L88.
- Jokipii, J. R., and B. Thomas (1981), Effects of drift on the transport of cosmic rays. IV - Modulation by a wavy interplanetary current sheet, *Astrophys. J.*, 243, 1115–1122.
- Jokipii, J. R., E. H. Levy, and W. B. Hubbard (1977), Effects of particle drift on cosmic-ray transport. I. General properties, application to solar modulation, *Astrophys. J.*, 213, 861–868.
- Kóta, J., and J. R. Jokipii (1983), Effects of drift on the transport of cosmic rays. VI - A three-dimensional model including diffusion, *Astrophys. J.*, 265, 573–581.
- Le Roux, J. A., and M. S. Potgieter (1995), The simulation of complete 11 and 22 year modulation cycles for cosmic rays in the heliosphere using a drift model with global merged interaction regions, *Astrophys. J.*, 442, 847–851.
- McDonald, F. B. (1998), Cosmic ray modulation in the heliosphere, *Space Sci. Rev.*, 83, 33–50.
- Parker, E. N. (1958), Dynamics of the interplanetary gas and magnetic fields, *Astrophys. J.*, 128, 664.
- Parker, E. N. (1965), The passage of energetic charged particles through interplanetary space, *Planet. Space Sci.*, 13(1), 9–49.
- Perko, J. S. (1987), Solar modulation of galactic antiprotons, *Astron. Astrophys.*, 184, 119–121.
- Potgieter, M. S. (1998), The modulation of galactic cosmic rays in the heliosphere: Theory and models, *Space Sci. Rev.*, 83, 158–174.
- Potgieter, M. S., and H. Moraal (1985), A drift model for the modulation of galactic cosmic rays, *Astrophys. J.*, 294, 425–440.
- Potgieter, M. S., J. A. Le Roux, L. F. Burlaga, and F. B. McDonald (1993), The role of merged interaction regions and drifts in the heliospheric modulation of cosmic rays beyond 20 AU: A computer simulation, *Astrophys. J.*, 403, 760–768.
- Scherer, K., H. Fichtner, and O. Stawicki (2002), Shielded by the wind: the influence of the interstellar medium on the environment of Earth, *J. Atmos. Sol. Terr. Phys.*, 64, 795–804.
- Toptygin, I. N. (1985), *Cosmic Rays in Interplanetary Magnetic Fields*, Kluwer Acad., Dordrecht, Netherlands.
- Usoskin, I. G., K. Alanko, K. Mursula, and G. A. Kovaltsov (2002), Heliospheric modulation strength during the neutron monitor era, *Sol. Phys.*, 207, 389–399.
- Usoskin, I. G., K. Alanko-Huotari, G. A. Kovaltsov, and K. Mursula (2005), Heliospheric modulation of cosmic rays: Monthly reconstruction for 1951–2004, *J. Geophys. Res.*, 110, A12108, doi:10.1029/2005JA011250.
- Yamada, Y., S. Yanagita, and T. Yoshida (1998), A stochastic view of the solar modulation phenomena of cosmic rays, *Geophys. Res. Lett.*, 25, 2353–2356.
- Zhang, M. (1999), A Markov stochastic process theory of cosmic-ray modulation, *Astrophys. J.*, 513, 409–420.

K. Alanko-Huotari and K. Mursula, Department of Physical Sciences, University of Oulu, POB 3000, FIN-90014, Oulu, Finland.

G. A. Kovaltsov, Ioffe Physical-Technical Institute, Politekhnikeskaya 26, RU-194021 St. Petersburg, Russia.

I. G. Usoskin, Sodankylä Geophysical Observatory (Oulu unit), University of Oulu, POB 3000, FIN-90014, Oulu, Finland. (ilya.usoskin@oulu.fi)